ChemPubSoc Europe

DOI: 10.1002/chem.201902481

CHEMISTRY A European Journal Full Paper

Macroscopic Structures

# A Hexanuclear Niobium Cluster Compound Crystallizing as Macroscopic Tubes

Jonas König and Martin Köckerling*[a]

**Abstract:** Compounds with ordered structures in one or two dimensions are exciting materials and investigated intensively in many different areas of science. Many activities have been put into the preparation of low-dimensional nano-scaled structures and many compounds in this size regime are known. Contrary, the number of known compounds that have low-dimensional macroscopic sized structures that form directly in a chemical reaction is very limited. Here, we present the synthesis of the niobium cluster compound $[(Et_2O)_2H]_2[Nb_6Cl_{18}]$, crystals of which grow in form of large hexagonal empty tubes of several centimeter length and diameters in the range of 2 mm. The single-crystal X-ray structure of this compound has been refined. Under warming, the compound readily eliminates diethyl ether molecules and decomposes. From a closer look at the crystallization process a step-by-step scheme of the procedure of the tube growth is proposed. The overall conclusion from this proposal is that a crucial balance between the cluster solution concentration, the crystal growth speed and the ether diffusion speed results in the formation of macroscopic crystal tubes.

## Introduction

Materials with anisotropic properties have attracted a huge amount of scientific and industrial interest. Anisotropic behavior related to low-dimensional structures has been and still is a very hot topic in many fields of science, especially physics. Low-dimensional compounds include nano-structured semiconductors, nanotubes, graphene and bio-minerals, besides others. With respect to new useful devices low-dimensional and nano-scaled semiconductors are investigated intensively.[1] In this area advanced CVD techniques allow for the preparation of the desired materials as nano-sized low-dimensional units.[2] Nanotubes, particularly carbon nanotubes are discussed for many different advanced applications and techniques. Examples include the formation of composite materials for high quality sport equipment like tennis racquets, baseball bats or bicycle frames, to strengthen light-weight alloys, for multifunctional coating materials, for microelectronics, for hydrogen storage, or to improve supercapacitors.[2b,3] Graphene, a two-dimensional planar sheet of carbon atoms, exhibits many unique properties such as outstanding electrical conductivity and a half-integer Quantum Hall effect. Furthermore, it exhibits great optical and mechanical properties.[4] In contrast to these examples of groups of materials with anisotropic properties, those of bio-minerals are different, because their anisotropy is important in the macroscopic (bulk) size, that is, for teeth and bones. The shape of such bio-minerals is considered to form through the crystallization of an inorganic main component into a composite material in the environment of other bio-organic compounds.[5] For the preparation of nano-sized low-dimensional materials various chemical methods have been developed, often described as top-down or bottom-up methods, besides physical methods, like the above mentioned CVD methods. The chemical preparation of macroscopic pieces of material with task-specific properties is still a challenge.

In this article we report about the synthesis of a hexanuclear cluster compound, which forms repeatable as millimeter-sized, that is, macroscopic tubes on crystallization, called cluster tubes.

## Results and Discussion

### Synthesis of macroscopic cluster tubes of $[(Et_2O)_2H]_2[Nb_6Cl_{18}]$ (1)

The preparation of **1** is done in three consecutive steps with an additional step of purification and crystallization. In the first step the starting material $K_4[Nb_6Cl_{18}]$ is produced in a high-temperature, solid state chemical reaction.[6] The reaction product is dissolved in water. By addition of $HCl_{(aq)}$ the compound $[Nb_6Cl_{14}(H_2O)_4]\cdot 4H_2O$ is precipitated and isolated in high yield and high purity.[7] For the preparation of **1** the compound $[Nb_6Cl_{14}(H_2O)_4]\cdot 4H_2O$ is treated with thionyl chloride in the presence of an excess of diethyl ether and 18-crown-6. All the

[a] J. König, Prof. Dr. M. Köckerling
Institute for Chemistry, Solid State Chemistry Group
University of Rostock, Albert-Einstein-Str. 3a, 18057 Rostock (Germany)
E-mail: Martin.Koeckerling@uni-rostock.de

The ORCID identification number(s) for the author(s) of this article can be found under: https://doi.org/10.1002/chem.201902481.

water ligands of the starting material are replaced by chloride ions and the co-crystallized $H_2O$ molecules removed. A two-electron oxidation of the cluster unit happens, as summarized in Scheme 1.[8]

$$[Nb_6Cl_{14}(H_2O)_4]\cdot 4H_2O + 10\ SOCl_2 + 4\ Et_2O \longrightarrow [(Et_2O)_2H]_2[Nb_6Cl_{18}] + 9\ SO_2 + 14\ HCl + SCl_2$$

**Scheme 1.** Overall reaction sequence for the preparation of the cluster tube compound **1**.

If the diethyl ether is introduced slowly by a diffusion process into the cluster solution in $SOCl_2$, as outlined in the Experimental Section, large, macroscopic, hexagonal tubes grow on the glass surface of the vials. In the earlier reaction attempts 18-crown-6 was present in the reaction mixture. It was repeatedly observed that on addition of 18-crown-6, which is not present in the final reaction product, large and well-shaped tubes were obtained. We assume that the added 18-crown-6 modifies the solubility and/or solution viscosity such that larges tubes form. Figure 1 shows a long side and a cross-section of such cluster tubes and Figure 2 a comparison of the size of a cluster tube with a two-cent euro coin.

It was possible to cut out a single crystal out of a tube and determine the single-crystal X-ray structure. Cluster compound **1** consists of the discrete hexanuclear niobium cluster anion $[Nb_6Cl_{18}]^{2-}$ and two diethyl ether coordinated $H^+$ ions, $[(Et_2O)_2H^+]$ (Et = ethyl, diethyl oxonium–diethyl etherate). The structure of one ion pair of this compound is shown in Figure 3.

Compound **1** crystallizes in the trigonal space group $P\bar{3}$ with one formula unit in the unit cell (for further details, including the CCDC information, see to the Experimental Section). The $[Nb_6Cl_{18}]^{2-}$ cluster unit is arranged around the Wyckoff site 1*a* with $\bar{3}$ symmetry. It resembles the "classical" $Nb_6Cl_{12}$-type transition-metal cluster with an all edge-bridged metal atom octahedron and one further halide ion on each vertex position.[9] In accordance with the $\bar{3}$ symmetry the Nb atoms within the two triangular planes of the trigonal antiprism with the same *z* coordinates are equilateral with a Nb–Nb distance of 3.0151(5) Å, whereas the distance between the Nb atoms between the two triangles is slightly longer, 3.0356(5) Å. The Nb–Cl distances of the edge-bridging halides Cl1 and Cl2 measure in average 2.4217 Å. That of the *exo*-directed Cl3 atom is found at 2.4779(9) Å. These values are in accordance with an two-electron oxidized cluster unit bearing 14 cluster-based electrons.[8]

The diethyl oxonium–diethyl etherate cation is located around the Wyckoff site 2*d* with threefold rotational symmetry. Because the $[(Et_2O)_2H^+]$ cation does not have this point symmetry it is disordered around this special position and refined using a split model with a 1/3 occupation of each part. The cation consists of two diethyl ether molecules and one $H^+$ ion, arranged such that the ether chains are oriented almost crosswise to each other, with one of the O atoms being protonated,

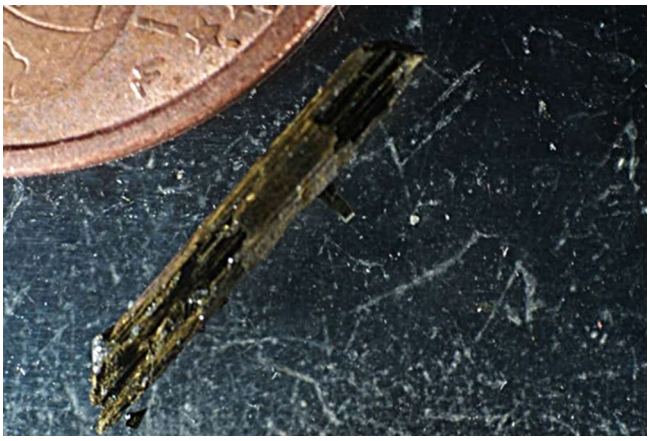

**Figure 2.** Size comparison of a cluster tube with a two-cent euro coin under the optical microscope (10-fold magnification).

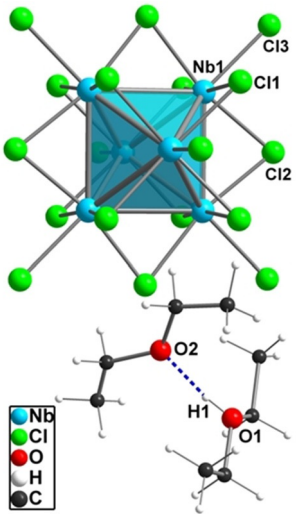


**Figure 3.** Structure of the cluster anion and the diethyl oxonium–diethyl etherate cation in crystals of **1**, with only one orientation of the threefold disordered cation shown.

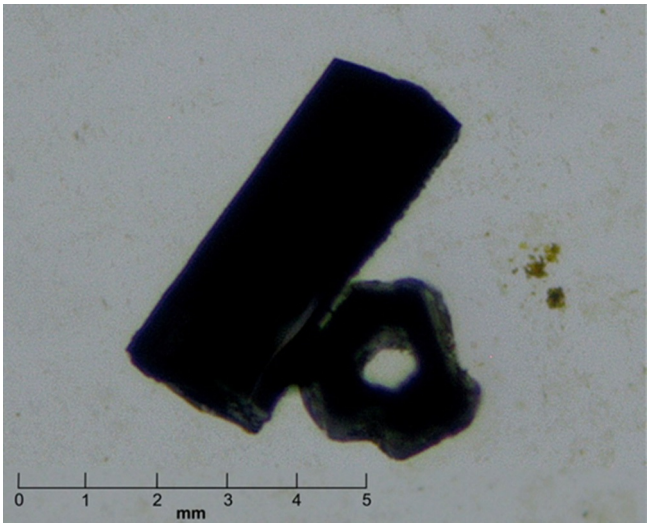


**Figure 1.** Light optical microscopic view of the macroscopic cluster tubes with 10-fold magnification along and perpendicular to the tube axis.

 

see Figure 3. The O atoms of the two neighboring diethyl ether molecules are 2.439(9) Å apart, what corresponds to a strong hydrogen bond. The arrangement of ions in and around the unit cell with only one of the three orientations of each protonated $Et_2O$ pair is shown in Figure 4.

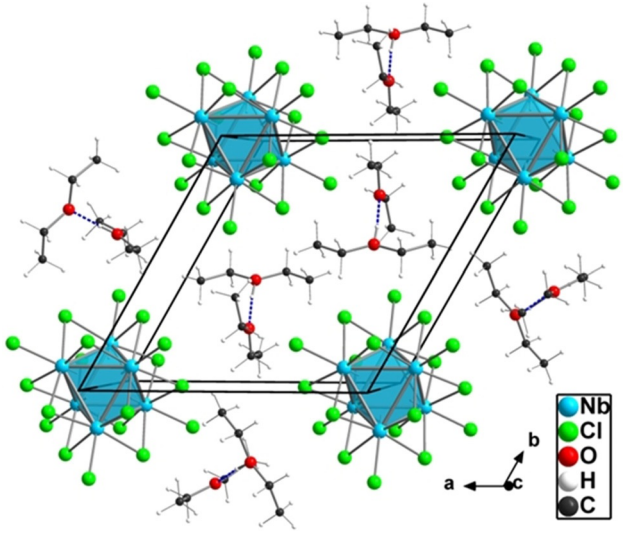


**Figure 4.** View of the content of the unit cell of **1**. Only one orientation of each disordered $[(Et_2O)_2H]^+$ cation is shown.

The existence of the protonated ether pairs is further proved by $^1$H NMR spectra, which show a singlet at 14.62 ppm in DMSO solution, which is indicative of a protonated DMSO species, obtained on dissolution by $H^+$ transfer from the ether-oxonium species to the DMSO molecules.[10] Ether-oxonium ions have been repeatedly used as cationic counter ions of interesting chemical species.[11] As with many of such compounds, **1** loses already at room temperature ether molecules and the compound decomposes. This is evident, for example, from the TG curve (thermogravimetry), shown together with the DSC curve in the range of room temperature up to 360 °C in Figure 5. The mass loss, starting at room temperature, reaches a plateau at around 140 °C at which the mass loss equals 19%, likely corresponds to the loss of all four diethyl ether molecules of the cation of the cluster compound [Eq. (1)]:

$$[(Et_2O)_2H][Nb_6Cl_{18}] \xrightarrow{\Delta} H_2[Nb_6Cl_{18}] + 4\,Et_2O \uparrow \quad (1)$$

Further decomposition happens at higher temperatures, which could go along with the loss of HCl molecules, as proposed for compounds with the same cluster anion and pyridineium cations earlier.[12] The easy loss of ether molecules and likely reorientation is also evident from the X-ray powder patterns, which show different patterns depending on the storage times of the samples before measurement. Nevertheless, if the storage time is short, the pattern, calculated from the values of the single crystal structure, is present in the pattern, besides others. Similar observations are done with the elemental analyses, which show different values depending on storage time. One example is given in the Experimental Section, in which the measured composition is in accordance with a sample, in which **1** has lost one molecule of $Et_2O$, that is, $[(Et_2O)_{1.5}H]_2[Nb_6Cl_{18}]$.

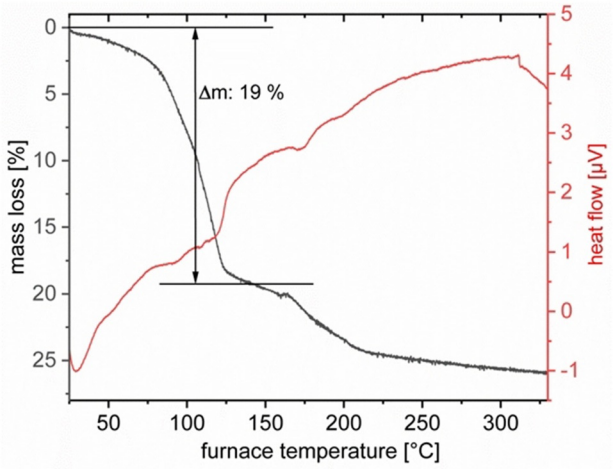


**Figure 5.** Thermogravimetric curve (black line) and DSC curve (red line), as observed on heating of **1** from room temperature to 350 °C. The arrow-indicated mass difference corresponds to the loss of four ether molecules of $[(Et_2O)_2H]_2[Nb_6Cl_{18}]$.

The most interesting feature of the title compound is, of course, the existence as macroscopic tubes. The following observations are used to derive a cluster tube formation model, which is depicted in Figure 6. 1) Cluster tube formation is (so far) only observed, when diethyl ether is used, not if other oxo-species that have the capability to form oxonium ions (for example THF), or if protonated N-bases are used. 2) The crystal growth always starts on the surface of the glass vial. 3) The crystals have a (often irregular) hexagonal shape. 4) The part of the crystals which is very close to the glass surface is completely filled (no tube) and has an increasing diameter (cone-shape) away from the glass surface. 5) After the initial compact growth the crystals become tubes. Figure 6 sketches the proposed step-by-step formation of the cluster tubes, as diethyl ether diffuses into the saturated solution of the cluster in $SOCl_2$. The green color indicates the saturated cluster solution and blue for the solution that contains dissolved $Et_2O$. As the ether concentration increases, a supersaturated layer (marked orange) is formed. At the glass surface within this layer crystal seeds form and initial crystal growth happens. At this stage the crystals have no tube form and are of regular hexagonal shape as sketched by the cross-section in Figure 6 A. The crystals have a preferred growth direction that coincides with the crystallographic *c* direction, along which they grow faster than in any other direction. As the crystal grows the supersaturated layer moves downward. At this initial crystal growth stage, the ether concentration around the crystal reduces and diffusion processes start to determine the further crystal growth. Because of the combination of ether diffusion speed, crystal growth speed and cluster diffusion speed, the crystal face, along which the crystal grows becomes oriented parallel to the liquid surface, see Figure 6 B. Thereby, the crystal cross-sec-

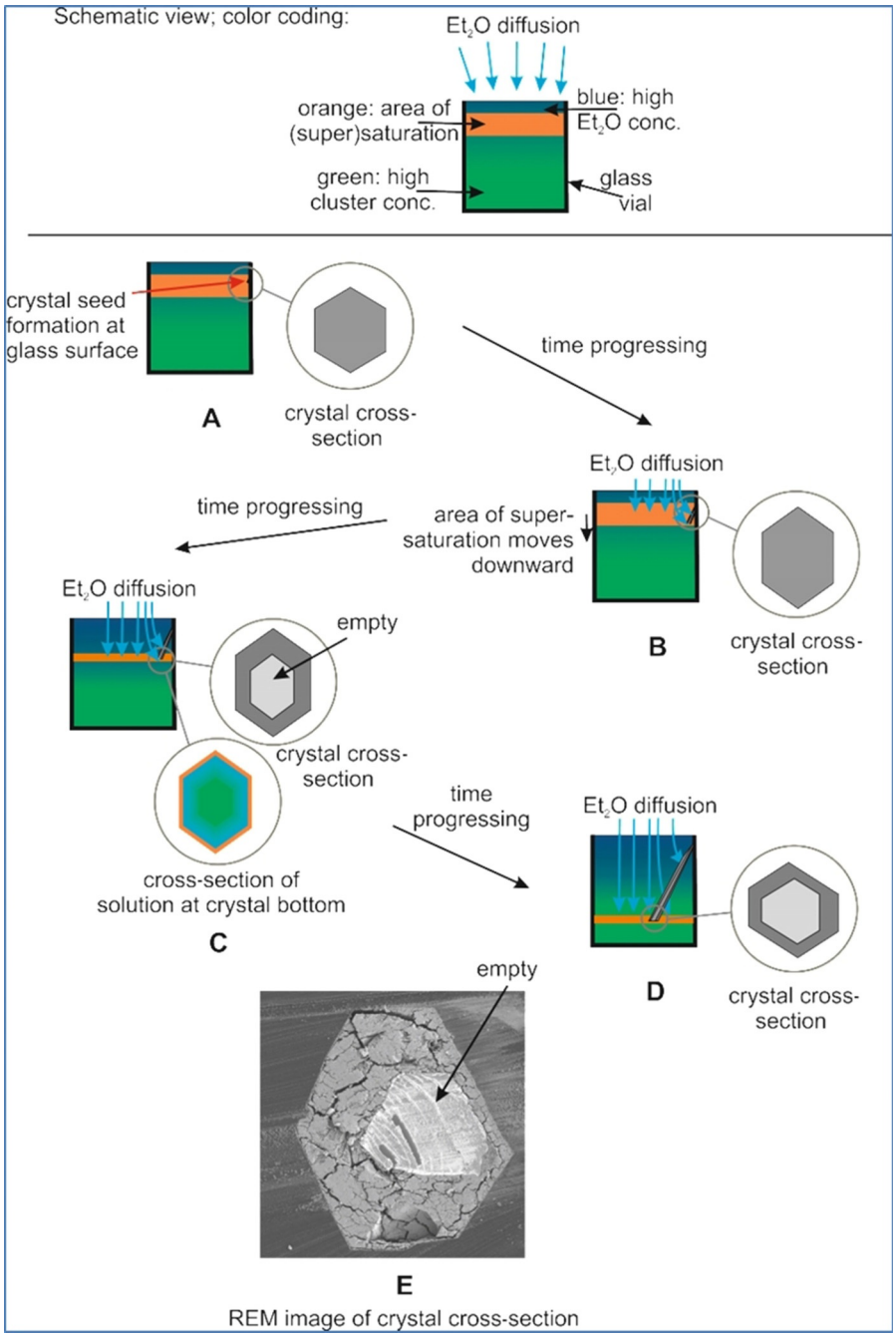


**Figure 6.** Proposed step-by-step procedure of the formation of macroscopic cluster tubes of $[(Et_2O)_2H]_2[Nb_6Cl_{18}]$.

tion becomes distorted from ideal hexagonal. With proceeding crystal growth, the cluster concentration reduces in the crystal growth area and the layer of supersaturation moves slowly down the glass vial (Figure 6B). Thereby the distance for the ether molecules to reach the crystal face with fastest growth (bottom of the crystal) increases. Because the supply with ether molecules at the crystal growth face is slower than the crystal growth, the supersaturation is quickly undercut. Since the ether molecules approach the crystal from top lateral and not from bottom, the crystal grows first at the surrounding (Figure 6C). At the point, where the ether diffusion speed falls behind the crystal growth speed, not enough ether molecules exist anymore inside of the crystal to have the crystal completely stuffed (see cross-section of the solution at the crystal bottom in Figure 6C). Thereby, the crystal becomes a tube as schematically depicted in Figure 6C (crystal cross-section). From that point on the crystal growth as macroscopic tube (Figure 6D). Figure 6E is a REM image of a crystal cross-section showing the empty inner part. The crystal cracks come from the separation of ether molecules during the crystal preparation for the REM measurements. Since the tubes grow inclined downwards and the crystal growth speed is higher than the cluster diffusion speed, the upper parts of the tubes are in a higher cluster concentration and the lower parts in a lower

 

concentration (what holds for the direct vicinity of the crystal), which results in a non-uniform tube cross-section.

Self-assembled macroscopic tubes have so far never been observed in cluster systems. The few examples known in other chemical systems are described in Ref. [13].

## Conclusions

We have developed a procedure to grow macroscopic crystalline tubes of a hexanuclear niobium cluster compound. Overall, it can be stated that a crucial balance between the cluster solution concentration, the crystal growth speed and the ether diffusion speed results in the formation of the macroscopic crystal tubes.

## Experimental Section

### General

Due to the air and moisture sensitivity of some of the reactants, the handling of the starting materials and of the cluster tube material was carried out under inert gas conditions or using Schlenk techniques. The starting material, $K_4[Nb_6Cl_{18}]$, was prepared in a high-temperature synthesis.[6] From this the compound $[Nb_6Cl_{14}(H_2O)_4]\cdot 4H_2O$ was obtained also through a literature known procedure.[7] Elemental analyses (C and H) were done using a Elementar vario MICRO cube device. $^1$H-NMR spectra were obtained with a Bruker AVANCE 300 II spectrometer and calibrated with respect to the solvent signal of [D$_6$]DMSO. Infrared spectra in the range of 4000–500 cm$^{-1}$ were obtained with a Nicolet 380 FT-IR spectrometer with a Smart Endurance ATR device. Differential scanning calorimetry and thermogravimetry measurements were performed with a Setaram Labsys instrument. The samples were heated slowly up to 400 °C. The heating rate for DSC and TG measurements was 3 K min$^{-1}$.

### Synthesis

In a vial of 12 mL volume with screw cap and Teflon seal, which is equipped with a magnetic stirrer, 50 mg (0.19 mmol) 18-crown-6, 4 mL thionyl chloride, and 50 mg (0.042 mmol) of $[Nb_6Cl_{14}(H_2O)_4]\cdot 4H_2O$ are placed. The cap is not screwed tightly, such that gases, which form in the chemical reaction, can lift off the cap and pass off. The mixture is stirred until all solid components are dissolved. The dark olive-green solution is allowed to stand unstirred for 2 hours. Then, it is divided equally into four volumes, which are transferred into vials of 7 mm inner diameter and 50 mm height. Each one is placed in an empty, larger vial of 14 mm inner diameter and 60 mm height. The outer vials are filled with diethyl ether ($Et_2O$) up to a height of approximately 10 mm. The cap of the outer vial is screwed tightly. Within a week the color of the cluster solution has faded into pale yellow and a large number of black crystals form on the glass surface. They are tubes with hexagonal cross-section. Under these conditions they reach lengths of up to 2.8 cm and diameters of up to 2 mm. Besides the black crystals some white precipitate is observed. The crystals are carefully detached from the glass surface of the vial using a glass fiber and quickly transferred together with the liquid phase into a thoroughly dried Schlenk bulb under argon atmosphere. The liquid phase is removed with a syringe and the crystals are treated several times with dried and degassed $Et_2O$ until all white side products are removed. To remove $SOCl_2$ what might be still present on the crystals, they are treated for up to 24 hours with anhydrous diethyl ether, which is treated with water after removal from the crystals. As long as the aqueous phase is acidic the procedure is repeated. Afterwards, the crystals are dried quickly in a slow stream of dry argon. They easily and quickly lose ether molecules, so that experimental elemental analysis and $^1$H NMR data differ from those calculated for $[(Et_2O)_2H]_2[Nb_6Cl_{18}]$.

Yield: 38 mg (76% with respect to the amount of used $[Nb_6Cl_{14}(H_2O)_4]\cdot 4H_2O$).

IR: (ATR, RT): $\tilde{\nu}$ = 744 (vs.); 885 (vs.); 999 (s); 1055 (m); 1134 (m); 1176 (s); 1234 (m); 1292 (m); 1379 (m); 1435 (m); 1518 (m); 2937 (w); 2983 cm$^{-1}$ (m).

Elemental analysis (%): Found: C, 11.24; H, 2.48;. calculated for $H_2[Nb_6Cl_{18}]\cdot 3.333\ Et_2O$: C, 11.27; H, 2.50. After storing outside of the vial under argon, found: C, 10.15; H, 2.27; calculated for $H_2[Nb_6Cl_{18}]\cdot 3\ Et_2O$: C, 10.25; H, 2.22.

$^1$H NMR: ([D$_6$]DMSO, RT): $\delta$ = 14.62 (s, 2.63 H), 3.38 (q, $J$ = 6.99 Hz, 16 H), 1.09 ppm (t, $J$ = 6.99 Hz, 24 H), (Integration of the number of hydrogen atoms in agreement with $[(Et_2O)_{1.5}H]_2[Nb_6Cl_{18}]$).

### Single crystal X-ray diffraction

The diffraction data was collected using a Bruker APEX-II CC diffractometer with a graphite monochromator, an Oxford-Cryosystems 700-Series-Cryostream-Cooler, and an Apex-Smart CCD detector. $Mo_{K\alpha}$ radiation, $\lambda$ = 0.71073 Å, was used. Intensity measurements, integration, and scaling of the data were performed with the respective Bruker software. For the multi-scan absorption corrections the program SADABS was used.[14] The Shelx-2014/1 software was used for solving and refining the structures.[15] All atoms except the hydrogen atoms were refined anisotropically. CCDC 1827247 contain the supplementary crystallographic data for this paper. These data are provided free of charge by The Cambridge Crystallographic Data Centre.

### X-ray powder diffraction

X-ray powder diffraction measurements were carried out with a Stoe Stadi P powder diffractometer with $Cu_{K\alpha 1}$ radiation ($\lambda$ = 1.5418 Å) using a linear PSD detector. Measurements were carried out in transmission setup. Data collection and handling was performed with the WinXPow program.[16]

## *Acknowledgements*

The authors thank Dr. A. Villinger (Universität Rostock) for taking care of the X-ray facilities. Financial support from the Deutsche Forschungsgemeinschaft (DFG) through the SPP 1708 is gratefully acknowledged (KO 1616/8-1 and -2).

## Conflict of interest

The authors declare no conflict of interest.

**Keywords:** cluster compounds · materials · niobium · structure elucidation · tubes

[1] *Semiconductor Nanotechnology: Advances in Information and Energy Processing and Storage* (Eds.: S. M. Goodnick, A. Korkin, R. Nemanich), Springer, Amsterdam, **2018**.

 

[2] a) *Micro and Nanomanufacturing, Vol. 2* (Ed.: M. J. Jackson, W. Ahmed), Springer, Amsterdam, **2017**; b) Y. Hu, *Carbon and Metal Oxides Based Nanomaterials for Flexible High Performance Asymmetric Supercapacitors*, Springer, Singapore **2018**.

[3] a) *Futuristic Composites: Behavior, Characterization, and Manufacturing* (Eds.: S. S. Sidhu, P. S. Bains, R. Zitoune, M. Yazdani), Springer Singapore, **2018**; b) M. F. L. De Volder, S. H. Tawfick, R. H. Baughman, A. J. Hart, *Science* **2013**, *339*, 535 – 539.

[4] a) M. K. Blees, A. W. Barnard, P. A. Rose, S. P. Roberts, K. L. McGill, P. Y. Huang, A. R. Ruyack, J. W. Kevek, B. Kobrin, D. A. Muller, P. L. McEuen, *Nature* **2015**, *524*, 204 – 207; b) T. Higuchi, C. Heide, K. Ullmann, H. B. Weber, P. Hommelhoff, *Nature* **2017**, *550*, 224 – 228; c) K. S. Novoselov, Z. Jiang, Y. Zhang, S. V. Morozov, H. L. Stormer, U. Zeitler, J. C. Maan, G. S. Boebinger, P. Kim, A. K. Geim, *Science* **2007**, *315*, 1379; d) P. Narang, L. Zhao, S. Claybrook, R. Sundararaman, *Adv. Opt. Mater.* **2017**, *5*, 1600914; e) K. S. Novoselov, A. Mishchenko, A. Carvalho, A. H. C. Neto, *Science* **2016**, *353*, aac9439.

[5] a) *Biomineralization and Biomaterials: Fundamentals and Applications, Vol. 104* (Ed.: C. Aparicio, M.-P. Ginebra), Elsevier, Cambridge, **2016**; b) *Biomineralization: From Nature to Application* (Eds.: A. Sigel, H. Sigel, R. K. O. Sigel), Wiley, Hoboken, **2008**.

[6] A. Simon, H. G. von Schnering, H. Schäfer, *Z. Naturforsch. B* **1968**, *361*, 235 – 248.

[7] F. W. Koknat, J. A. Parson, A. Vongvusharintra, *Inorg. Chem.* **1974**, *13*, 1699 – 1702.

[8] J. König, I. Dartsch, A. Topp, E. Guillamón, R. Llusar, M. Köckerling, *Z. Anorg. Allg. Chem.* **2016**, *642*, 572 – 578.

[9] a) H. S. Harned, C. Pauling, R. B. Corey, *J. Am. Chem. Soc.* **1960**, *82*, 4815 – 4817; b) A. Simon, *Angew. Chem. Int. Ed. Engl.* **1988**, *27*, 159 – 183; *Angew. Chem.* **1988**, *100*, 163 – 188; c) H. Schäfer, H. G. von Schnering, *Angew. Chem.* **1964**, *76*, 833 – 849.

[10] M. Hopfinger, K. Lux, A. Kornath, *ChemPlusChem* **2012**, *77*, 476 – 481.

[11] a) I. Krossing, I. Raabe, *Angew. Chem. Int. Ed.* **2004**, *43*, 2066 – 2090; *Angew. Chem.* **2004**, *116*, 2116 – 2142; b) M. Brookhart, B. Grant, A. F. Volpe, *Organometallics* **1992**, *11*, 3920 – 3922; c) P. Jutzi, C. Müller, A. Stammler, H.-G. Stammler, *Organometallics* **2000**, *19*, 1442 – 1444.

[12] B. Spreckelmeyer, C. Brendel, M. Dartmann, H. Schäfer, *Z. Anorg. Allg. Chem.* **1971**, *386*, 15 – 26.

[13] a) S. Tragl, K. Gibson, J. Glaser, V. Duppel, A. Simon, H.-J. Meyer, *Z. Anorg. Allg. Chem.* **2006**, *632*, 2125; b) S. Tragl, K. Gibson, J. Glaser, V. Duppel, A. Simon, H. J. Meyer, *Solid State Commun.* **2007**, *141*, 529 – 534; c) J. Wu, L. Zhao, L. Zhang, X. L. Li, M. Guo, A. K. Powell, J. Tang, *Angew. Chem. Int. Ed.* **2016**, *55*, 15574 – 15578; *Angew. Chem.* **2016**, *128*, 15803 – 15807; d) M. Remskar, Z. Skraba, F. Cléton, R. Sanjinés, F. Lévy, *Appl. Phys. Lett.* **1996**, *69*, 351 – 353; e) W. Liao, Y. Li, X. Wang, Y. Bi, Z. Su, H. Zhang, *Chem. Commun.* **2009**, 1861 – 1863; f) S. Mardix, *J. Appl. Crystallogr.* **1984**, *17*, 328 – 330; g) D. H. Mash, F. Firth, *J. Appl. Phys.* **1963**, *34*, 3636 – 3637; h) J. J. Pagano, T. Bansagi, Jr., O. Steinbock, *Angew. Chem. Int. Ed.* **2008**, *47*, 9900 – 9903; *Angew. Chem.* **2008**, *120*, 10048 – 10051; i) Q. Xu, Y. Yuan, J. Yi, C. Ma, *Solid State Sci.* **2007**, *9*, 732 – 736.

[14] L. Krause, R. Herbst-Irmer, G. M. Sheldrick, D. Stalke, *J. Appl. Crystallogr.* **2015**, *48*, 3 – 10.

[15] a) G. M. Sheldrick, *Acta Crystallogr. Sect. A* **2008**, *64*, 112 – 122; b) G. M. Sheldrick, *Acta Crystallogr. Sect. A* **2015**, *71*, 3 – 8.

[16] WinXPOW (vers. 2.25), Stoe & Cie GmbH, Darmstadt, Germany, **2009**.

Manuscript received: May 30, 2019
Revised manuscript received: July 8, 2019
Accepted manuscript online: July 12, 2019
Version of record online: September 30, 2019

 